Science Advances
AAAS

Supplementary Materials for

Ionic communication for implantable bioelectronics

Zifang Zhao, George D. Spyropoulos, Claudia Cea, Jennifer N. Gelinas*, Dion Khodagholy*

*Corresponding author. Email: jng2146@cumc.columbia.edu (J.N.G.); dk2955@columbia.edu (D.K.)

Published 6 April 2022, *Sci. Adv.* **8**, eabm7851 (2022)
DOI: 10.1126/sciadv.abm7851

The PDF file includes:

Other Supplementary Material for this manuscript includes the following:

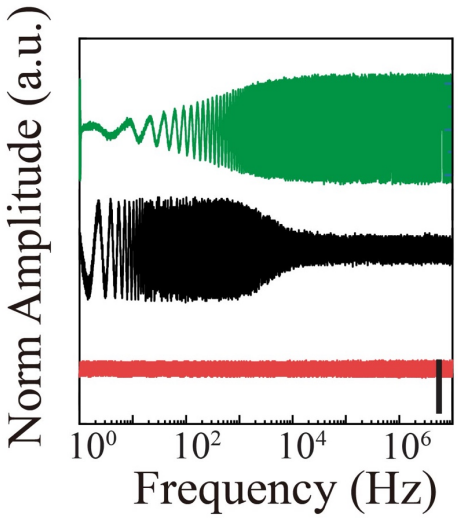

Supplementary Figure 1: Frequency response of IC in different media.

Differentially acquired frequency-sweep signal in PBS (green), DI (black), and IPA (red). IC electrode geometry: L = 25 mm, W = 25 mm, D = 25 mm. Scale bar 0.5 V/V.

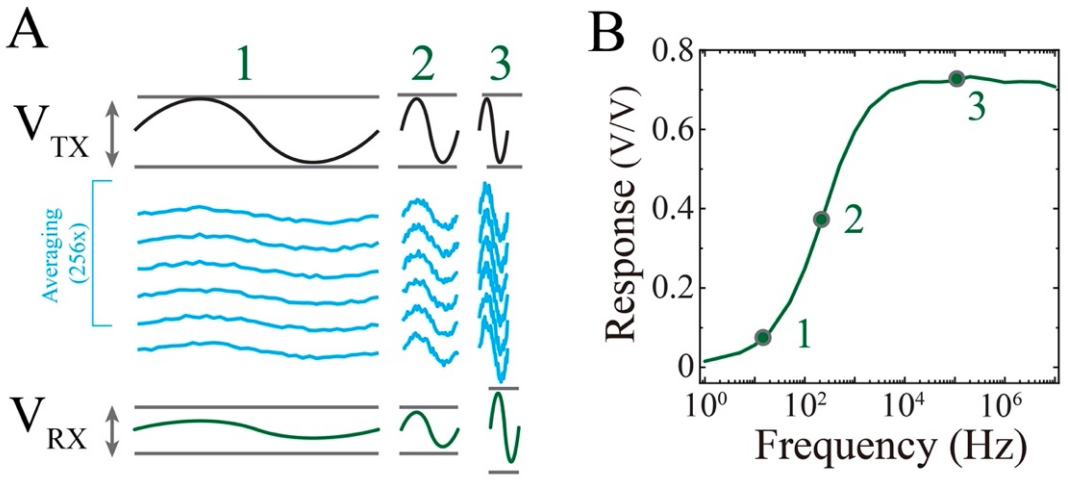

Supplementary Figure 2: IC frequency-response measurement and extraction protocol.

A) For each frequency, 256 cycles are generated at TX and acquired at RX electrode arrays. The peak-to-peak V_{RX} is then measured per cycle, averaged and divided by peak-to-peak V_{TX}.

B) Extraction of frequency-dependent response from measurements in (A). Numerals 1, 2, and 3 mark the frequencies shown in the sample frequency responses in (A).

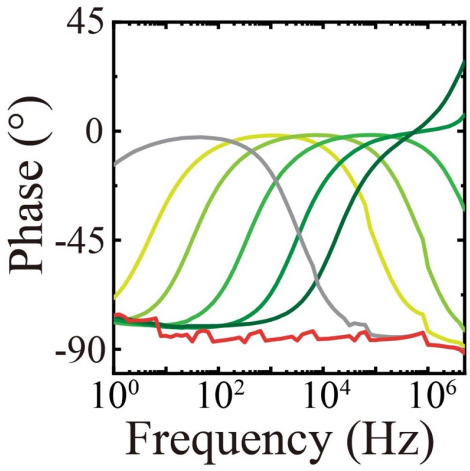

Supplementary Figure 3: Electrochemical impedance characterization of different media.

Corresponding phase spectrum of the electrochemical impedance spectrum shown in **Figure 1c**. Responses in various media (10^{-3}, 10^{-2}, 10^{-1} and 1× PBS (darker shades of green represent higher concentrations), deionized water (DI; gray) and isopropanol (IPA; red)) to a 1 Hz – 10MHz V_{TX} sweep signal. Interelectrode spacing between TX and RX electrodes, as well as distance between TX and RX arrays was fixed at 25 mm.

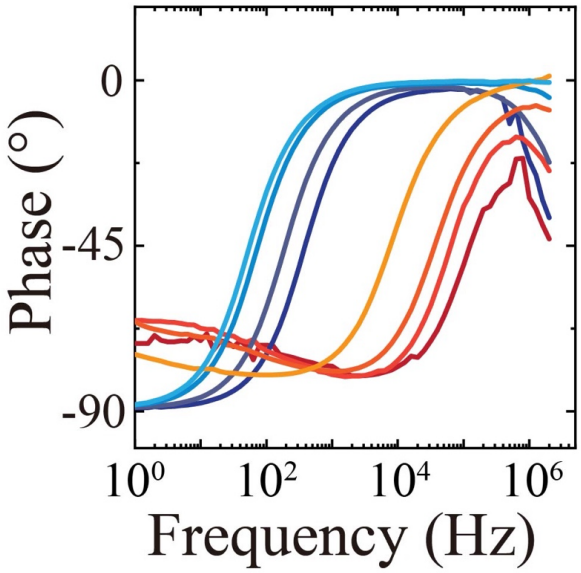

Supplementary Figure 4: Electrochemical impedance characterization for varying electrode size and material.

Corresponding phase spectrum of the electrochemical impedance spectrum shown in **Figure 3a** for conducting polymer-based (shades of blue) and Au-based (shades of red) IC electrodes with 5, 10, 20, 40 mm length (darker shades represent smaller lengths).

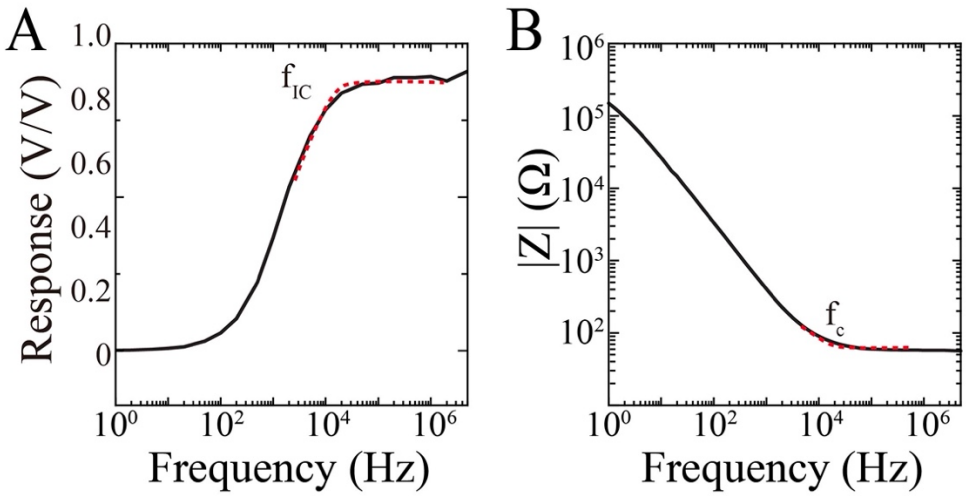

Supplementary Figure 5: Relationship of IC frequency (f_{IC}) and the electrochemical impedance corner frequency (f_C).

A) Frequency response of the IC electrodes shown in **Figure 3b** with labeled (f_{IC}).

B) The impedance magnitude of the IC electrode shown in (A) with labeled (f_C).

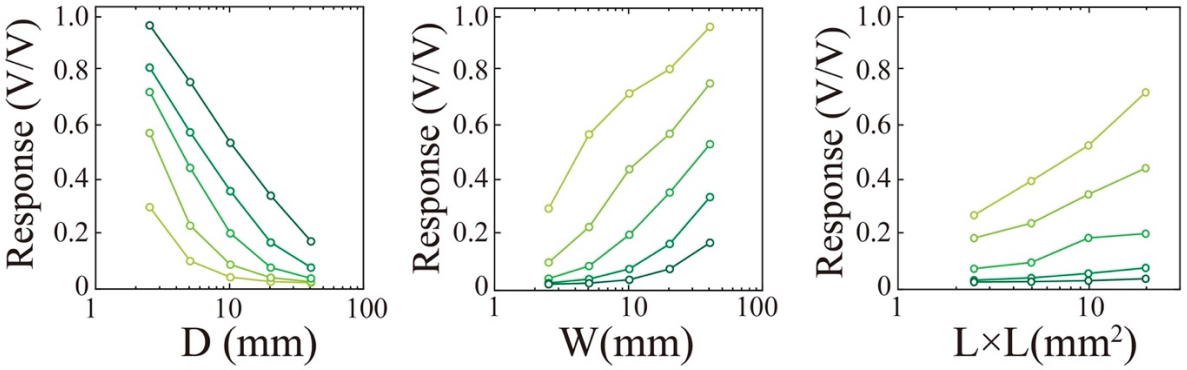

Supplementary Figure 6: Effect of electrode geometry (W, D and L) on IC response at frequencies above F_{IC}.

A) Response as a function of distance between RX and TX arrays (D). The superimposed lines show devices with 40, 20, 10, 5, and 2 mm distance between electrodes in a pair (W; darker shades represent larger distances).

B) Response as a function of distance between electrodes in a pair (W). The superimposed lines show devices with 40, 20, 10, 5, and 2 mm distance between RX and TX arrays (D; darker shades represent larger distances).

C) Response as a function of electrode area denoted as square electrode length (L). The superimposed lines show devices with 40, 20, 10, 5, and 2 mm distance between RX and TX arrays (D; darker shades represent larger distances).

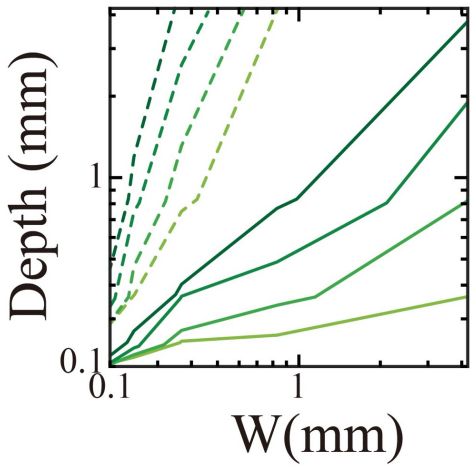

Supplementary Figure 7: IC implantation depth as a function of receiver's sensitivity and distance between electrodes in a pair (W).

Maximal implantation depth of IC as a function of electrode pair width (W). Electrode size: 2.5, 5, 10, 20 mm^2 (light to dark green). Solid lines highlight -20 dB signal attenuation while dashed lines indicate -40 dB.

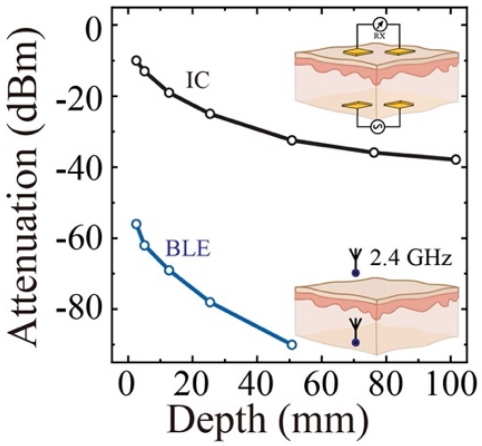

Supplementary Figure 8: Comparison of IC with 2.4 GHz RF-based communication.

Direct comparison of signal attenuation as a function of communication distance between IC (1 mm electrode length) and Bluetooth Low Energy (BLE) technology. The RF-based system had a dramatically higher signal attenuation (-50 dB) in physiological environments even at short distances and was not able to establish a link at distances further than 50 mm.

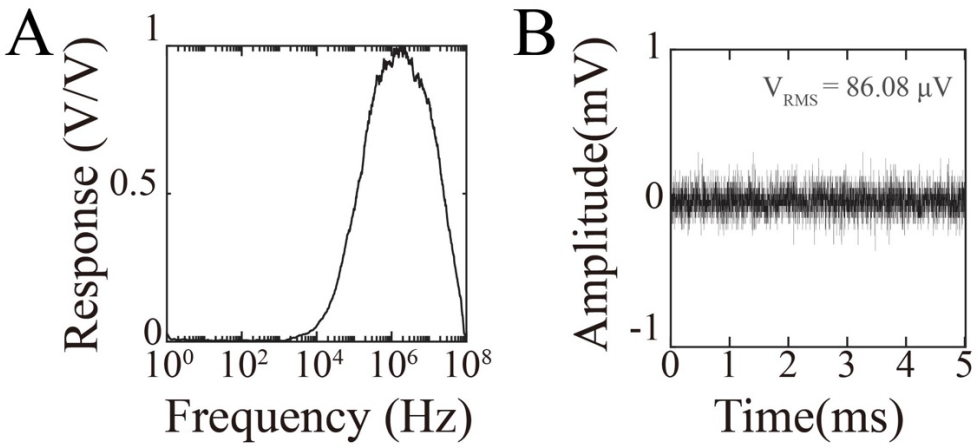

Supplementary Figure 9: Electrical characteristics for IC receiver amplifier.

A) RX bandpass filter profile tuned to 1–10 MHz frequencies.

B) Sample time traces showing the noise floor of receiver's amplifying circuit.

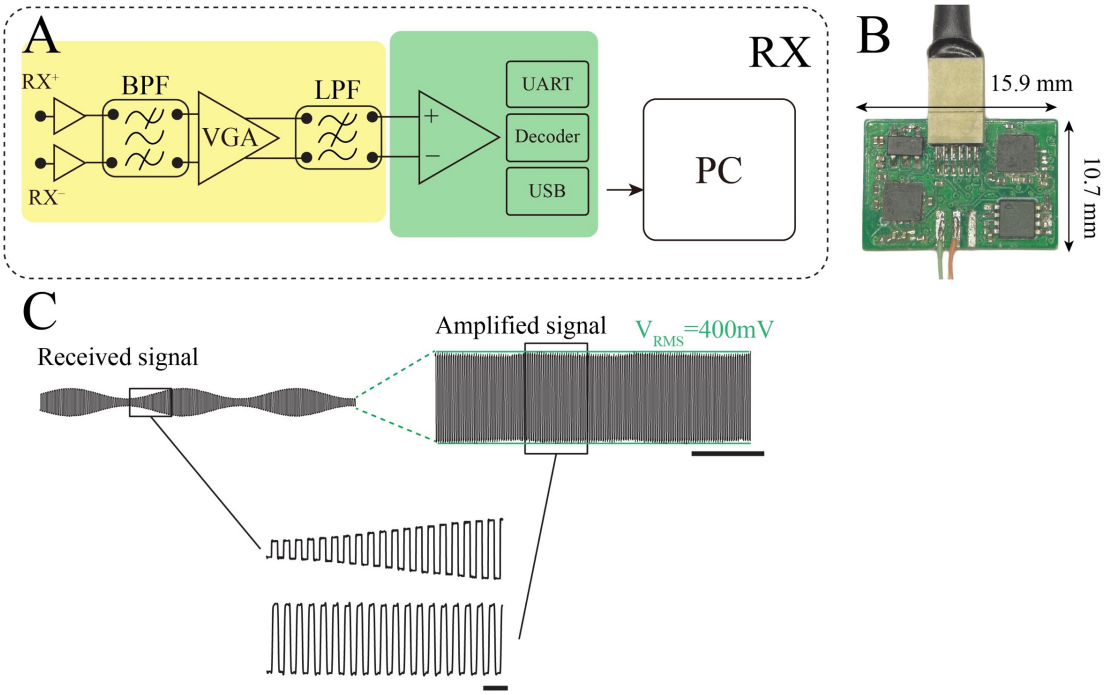

Supplementary Figure 10: IC receiver circuit, board level implementation, and its operation.

A) Schematic of IC receiver (RX) circuit. Yellow box: high gain-bandwidth amplifier with band-pass filter (BPF), variable gain amplifier (VGA) and low pass filter (LPF). Green box: data slicer with high-speed comparator, UART receiver, decoder and Universal Serial Bus (USB).

B) Micrograph of an IC RX circuit developed using off the shelf electronic components.

C) Illustration of VGA operation. The input signal (left) is a variable amplitude square pulse train resembling amplitude drifts caused by mechanical movements. The output (right) of the VGA is the corresponding fixed amplitude and amplified signal that is ready for slicing and digitization; scale bar 10 µs. The bottom traces show a zoomed version of the top streams; scale bar 1 µs.

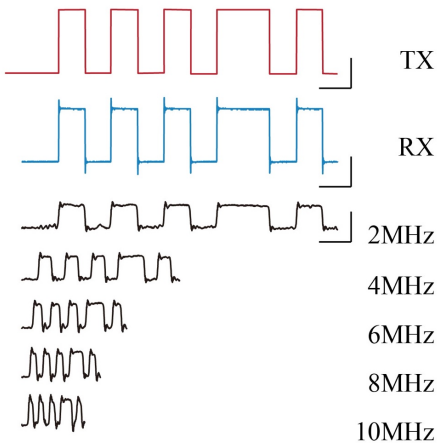

Supplementary Figure 11: Characterization of received signal at RX prior to digitization at different frequencies.

Red digital trace is the digital stream transmitted by TX. Blue trace is the output of VGA at RX prior to digitization; the RX was able to recover data up to 10MHz. Black traces show the VGA output at different frequencies.

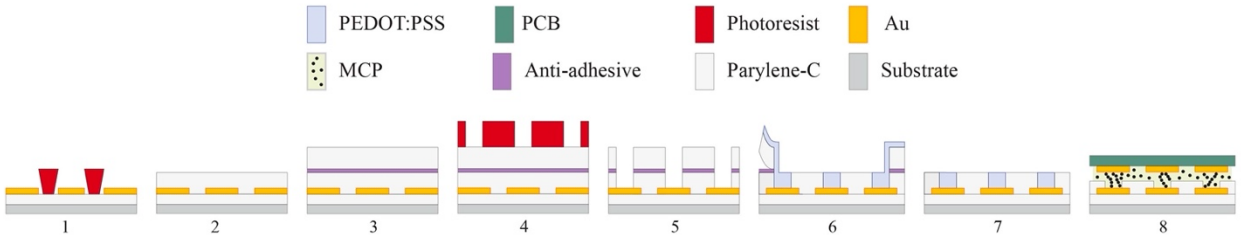

Supplementary Figure 12: Fabrication process of conformable IC transmitters.

1) Patterning of Au electrodes and interconnects via photolithography and a lift-off process; 2) deposition of parylene-C layer; 3) coating of an anti-adhesive layer and deposition of sacrificial parylene-C layer; 4) opening of the electrode sensing areas via successive photolithography; 5) plasma etching steps; 6) coating of PEDOT:PSS channel and peeling-off the sacrificial parylene-C layer; 7) final probe; 8) bonding the printed circuit board (PCB) through organic mixed-conducting particulate composite material (MCP).

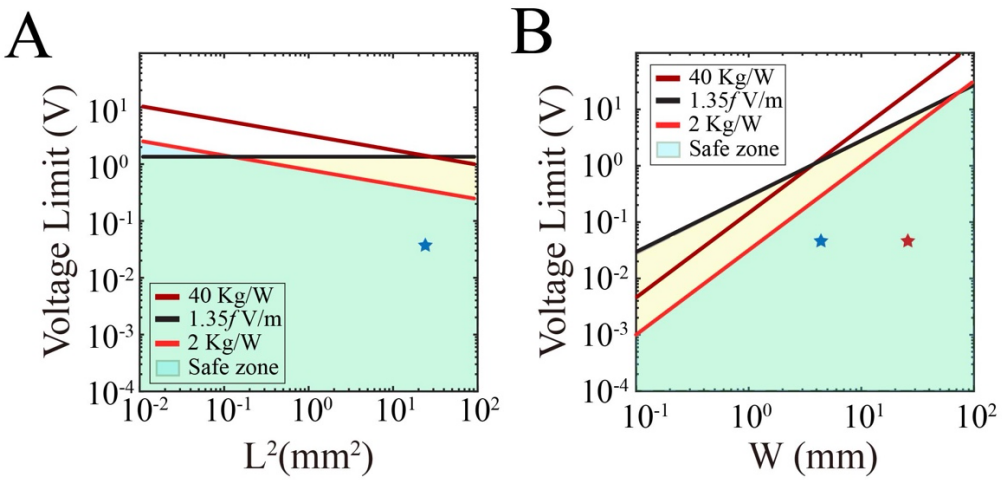

Supplementary Figure 13: IC does not exceed safe values for tissue specific energy absorption rate (SAR) as mandated by the International Commission on Non-Ionizing Radiation Protection (ICNIRP)(*42*).

A) Maximum operating voltage of IC as a function of TX electrode area. The red lines demarcates the occupational exposure limit while orange line indicates the limit based on general public exposure guidelines for head/torso. The black line indicates the safety boundary for the induced electric field in the tissue. The green shaded area highlights the compliant voltages for a given electrode area. The star indicates the parameters used in our *in vivo* studies (V_{TX} = 30 mV, L = 5 mm)

B) Maximum operating voltage of IC as a function of TX interelectrode distance. Colored lines represent safety limits as in (A). Stars indicate the parameters used in our *in vivo* studies (V_{TX} = 30 mV, W = 5 and 20 mm).

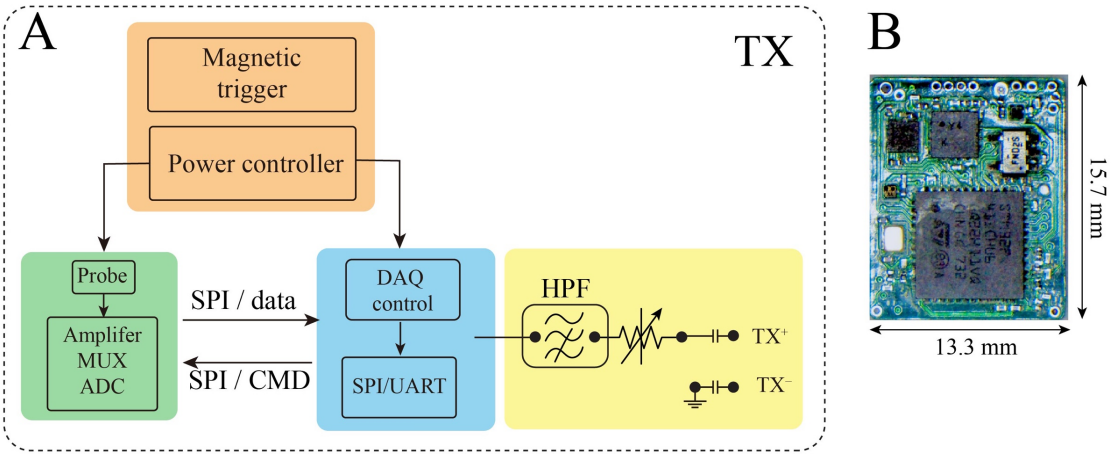

Supplementary Figure 14: IC transmitter circuit and board level implementation.

A) Schematic of implanted portion of IC-based neural interface device. Orange box: system power control. Green box: acquisition system with multiplexer (MUX) and analog-to-digital controller (ADC). Blue box: data acquisition control with serial-peripheral interface (SPI) and universal asynchronous receiver-transmitter (UART). Yellow box: IC transmitter circuit with high-pass filter (HPF) and voltage divider.

B) Micrograph of an IC TX developed using off the shelf electronic components.

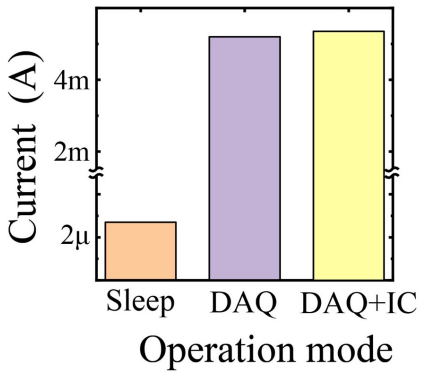

Supplementary Figure 15: Power consumption of implanted IC-based neural interface device.

Average current consumption measured by a source measure unit (SMU) in different device states. In sleep state, the microcontroller (µC) is in power saving mode, awaiting the external trigger in the form of the applied magnet. In the DAQ state, the Intan microchip is activated and digital data in the form of a low-voltage differential signal (VDS) is generated and regulated by the µC. In the DAQ+IC state, the LVDS data is transformed into Manchester code and attenuated 100 times ($30mV_{P-P}$) using the µC and external circuitry.

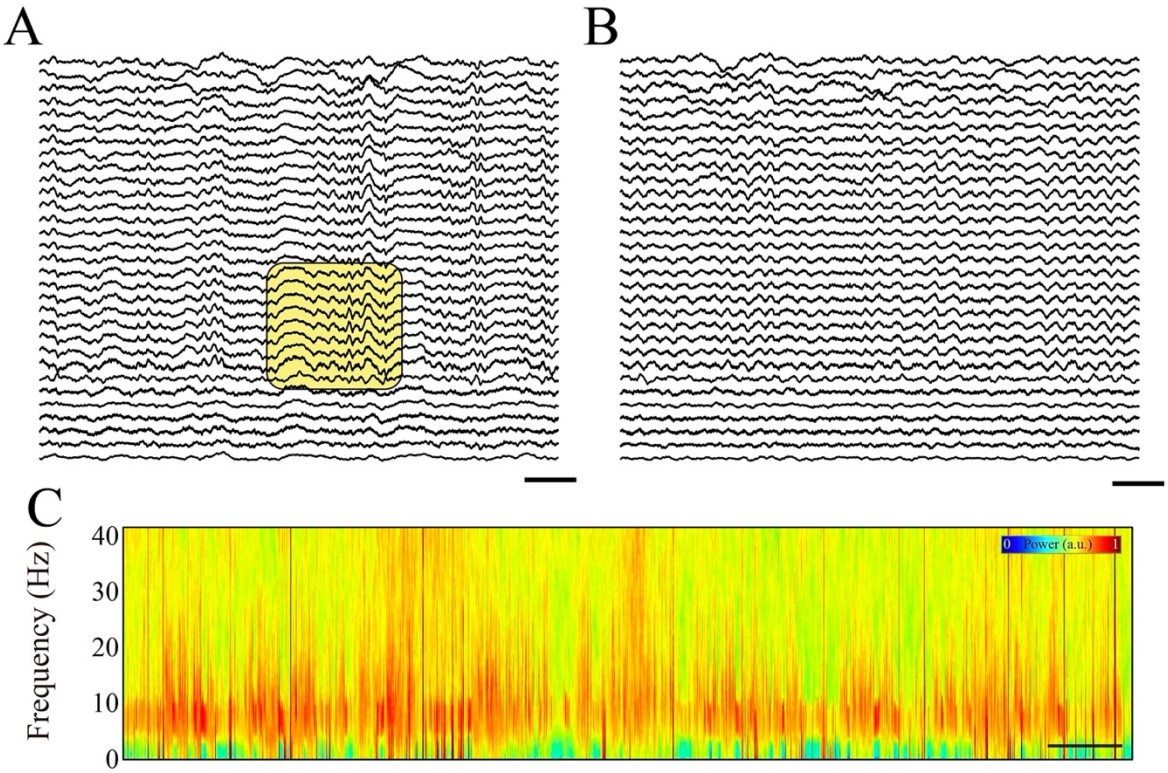

Supplementary Figure 16: Sample raw LFP traces and spectrogram of cortical activity transmitted by IC.

A) Raw LFP traces acquired during NREM sleep in a freely moving rat. The highlighted region marks a slow wave followed by a sleep spindle; scale bar 200 ms.

B) Raw LFP traces acquired during REM sleep in a freely moving rat with visible theta band (5-8 Hz) activity; scale bar 200 ms.

C) Continuous time-frequency spectrogram of more than 10 h of LFP transmitted by IC from a freely moving rat. Warmer colors represent higher power content in arbitrary units (a.u.); scale bar 1 h.

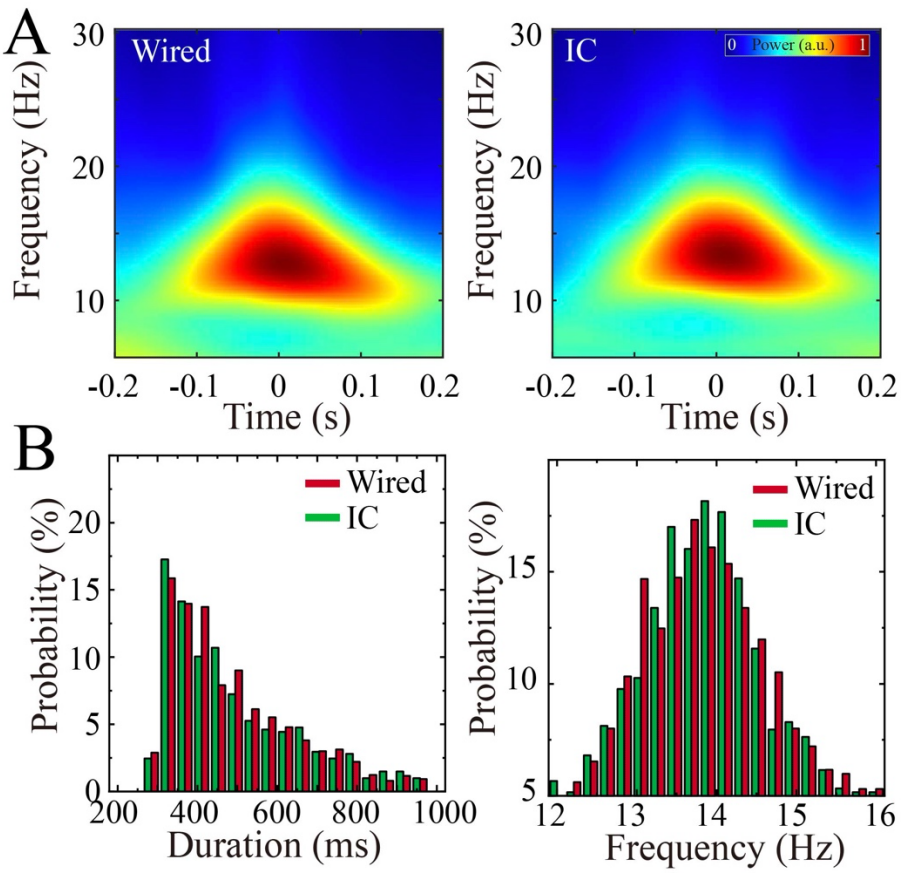

Supplementary Figure 17: Direct comparison of characteristic neural oscillations transmitted by IC and wired communication in freely moving rats.

A) Trigger-averaged time-frequency spectrogram at the time of detected thalamocortical sleep spindles revealed similar frequency content between IC and wired communication.

B) Distributions of duration (left) and mean frequency (right) of detected thalamocortical sleep spindles between IC and wired communication did not reveal significant differences (n = 608 spindles, Kolmogorov-Smirnov test; $p = 0.39$ (duration), $p = 0.32$ (mean frequency)).

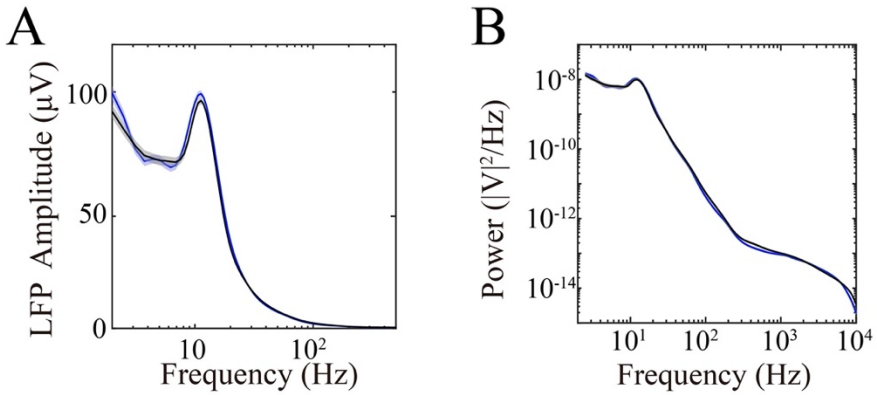

Supplementary Figure 18: Spectral comparison of neural signals transmitted by IC and wired communication in freely moving rats.

A) Power spectra centered on detected sleep spindles during NREM transmitted using IC (blue) and wired communication (black) revealed similar spectral profiles (n = 2239 spindle events).

B) Power spectral density from data transmitted using IC (blue) and wired communication (black) revealed similar spectral profiles. IC did not introduce substantial noise at any physiologic frequency compared to wired communication.

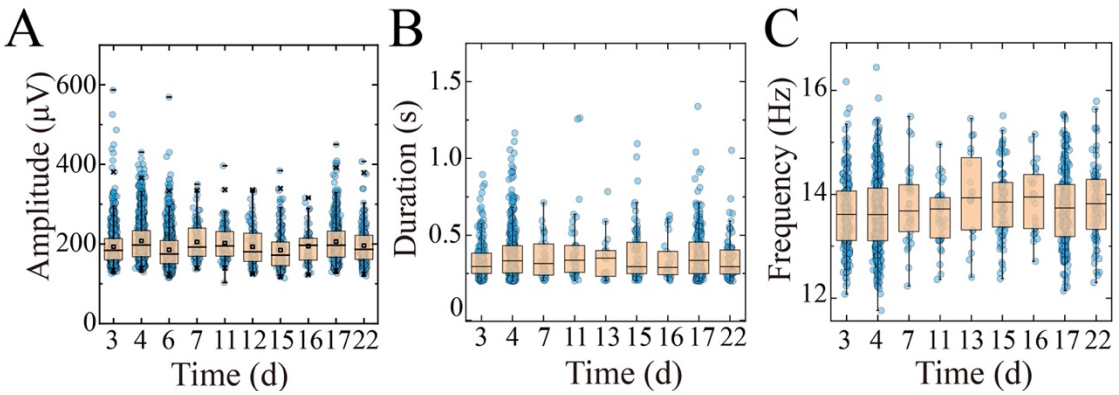

Supplementary Figure 19: IC maintained stable neural signal transmission over at least 3 weeks.

A) Amplitude distribution of thalamocortical sleep spindles transmitted by IC was stable across 22 days of recording.

B) Duration distribution of thalamocortical sleep spindles transmitted by IC was stable across 22 days of recording.

C) Frequency distribution of thalamocortical sleep spindles transmitted by IC was stable across 22 days of recording.

Technology	Bitrate (bps)	Consumption (W)	Power efficiency (bps/W)	Reference
IC	6×10^{6}	9×10^{-7}	6.6×10^{12}	This work
ME	5×10^{5}	1.2×10^{-4}	4.17×10^{9}	(*7*)
ME	7.2×10^{6}	3.28×10^{-1}	2.19×10^{7}	(*50*)
ME	4×10^{2}	3.95×10^{-1}	8.08×10^{2}	(*10*)
RF	4×10^{3}	3×10^{-5}	1.3×10^{8}	(*51*)
RF	4.8×10^{7}	8.91×10^{-2}	5.39×10^{8}	(*15*)
RF	2.56×10^{6}	5.6×10^{-3}	4.57×10^{8}	(*52*)
RF	2.4×10^{7}	9.06×10^{-2}	2.65×10^{8}	(*9*)
RF	2.4×10^{7}	1.42×10^{-1}	1.69×10^{8}	(*53*)
RF	2×10^{6}	1.44×10^{-2}	1.39×10^{8}	(*54*)
RF	2×10^{6}	1.5×10^{-2}	1.33×10^{8}	(*55*)
RF	5.12×10^{7}	5.61×10^{-1}	9.13×10^{7}	(*56*)
RF	1×10^{6}	1.2×10^{-2}	8.33×10^{7}	(*57*)
RF	3.5×10^{5}	1×10^{-2}	3.5×10^{7}	(*58*)
RF	1×10^{6}	3.5×10^{-2}	2.86×10^{7}	(*59*)
RF	1×10^{6}	5×10^{-2}	2×10^{7}	(*60*)
RF	1×10^{7}	6.45×10^{-1}	1.55×10^{7}	(*4*)
RF	1.96×10^{6}	1.72×10^{-1}	1.14×10^{7}	(*14*)
RF	6.4×10^{5}	1.13×10^{-1}	5.66×10^{6}	(*61*)
RF	3.2×10^{3}	5×10^{-3}	6.4×10^{5}	(*62*)
RF	2.05×10^{5}	9.2×10^{-5}	2.23×10^{9}	(*63*)

Supplementary Table 1: Performance specifications of IC, RF and ultrasound-based devices in Figure 6b.

Supplementary Video 1: Rat with fully implanted IC device and RX array attached navigates freely on an open field maze. Note that this rat is also implanted with hardware for connection of SPI cable to directly compare signals transmitted by IC and wired communication.

REFERENCES AND NOTES

1. E. Krook-Magnuson, J. N. Gelinas, I. Soltesz, G. Buzsáki, Neuroelectronics and biooptics: Closed-loop technologies in neurological disorders. *JAMA Neurol.* **72**, 823–829 (2015).

2. P. Jastrzebska-Perfect, S. Chowdhury, G. D. Spyropoulos, Z. Zhao, C. Cea, J. N. Gelinas, D. Khodagholy, Translational neuroelectronics. *Adv. Funct. Mater.* **30**, 1909165 (2020).

3. T. Someya, Z. Bao, G. G. Malliaras, The rise of plastic bioelectronics. *Nature* **540**, 379–385 (2016).

4. T. A. Szuts, V. Fadeyev, S. Kachiguine, A. Sher, M. V. Grivich, M. Agrochão, P. Hottowy, W. Dabrowski, E. V. Lubenov, A. G. Siapas, N. Uchida, A. M. Litke, M. Meister, A wireless multi-channel neural amplifier for freely moving animals. *Nat. Neurosci.* **14**, 263–269 (2011).

5. S. M. Won, L. Cai, P. Gutruf, J. A. Rogers, Wireless and battery-free technologies for neuroengineering. *Nat. Biomed. Eng.* 10.1038/s41551-021-00683-3 (2021).

6. C. Y. Kim, M. J. Ku, R. Qazi, H. J. Nam, J. W. Park, K. S. Nam, S. Oh, I. Kang, J. H. Jang, W. Y. Kim, J. H. Kim, J. W. Jeong, Soft subdermal implant capable of wireless battery charging and programmable controls for applications in optogenetics. *Nat. Commun.* **12**, 535 (2021).

7. D. Seo, R. M. Neely, K. Shen, U. Singhal, E. Alon, J. M. Rabaey, J. M. Carmena, M. M. Maharbiz, Wireless recording in the peripheral nervous system with ultrasonic neural dust. *Neuron* **91**, 529–539 (2016).

8. D. K. Piech, B. C. Johnson, K. Shen, M. M. Ghanbari, K. Y. Li, R. M. Neely, J. E. Kay, J. M. Carmena, M. M. Maharbiz, R. Muller, A wireless millimetre-scale implantable neural stimulator with ultrasonically powered bidirectional communication. *Nat. Biomed. Eng.* **4**, 207–222 (2020).

9. D. A. Borton, M. Yin, J. Aceros, A. Nurmikko, An implantable wireless neural interface for recording cortical circuit dynamics in moving primates. *J. Neural Eng.* **10**, 026010 (2013).

10. P. Jin, J. Fu, F. Wang, Y. Zhang, P. Wang, X. Liu, Y. Jiao, H. Li, Y. Chen, Y. Ma, X. Feng, A flexible, stretchable system for simultaneous acoustic energy transfer and communication. *Sci. Adv.* **7**, abg2507 (2021).

11. L. J. Challis, Mechanisms for interaction between RF fields and biological tissue. *Bioelectromagnetics* **26**, S98–S106 (2005).

12. E. R. Adair, R. C. Petersen, Biological effects of radiofrequency/microwave radiation. *IEEE Trans. Microw. Theory Tech.* **50**, 953–962 (2002).

13. IEEE Standard for Safety Levels with Respect to Human Exposure to Radio Frequency Electromagnetic Fields, 3 kHz to 300 GHz. **16**, 1–83 (1999).

14. A. Zhou, S. R. Santacruz, B. C. Johnson, G. Alexandrov, A. Moin, F. L. Burghardt, J. M. Rabaey, J. M. Carmena, R. Muller, A wireless and artefact-free 128-channel neuromodulation device for closed-loop stimulation and recording in non-human primates. *Nat. Biomed. Eng.* **3**, 15–26 (2019).

15. M. Yin, D. A. Borton, J. Komar, N. Agha, Y. Lu, H. Li, J. Laurens, Y. Lang, Q. Li, C. Bull, L. Larson, D. Rosler, E. Bezard, G. Courtine, A. V. Nurmikko, Wireless neurosensor for full-spectrum electrophysiology recordings during free behavior. *Neuron* **84**, 1170–1182 (2014).

16. A. Khalifa, Y. Karimi, Q. Wang, S. Garikapati, W. Montlouis, M. Stanacevic, N. Thakor, R. Etienne-Cummings, The microbead: A highly miniaturized wirelessly powered implantable neural stimulating system. *IEEE Trans. Biomed. Circuits Syst.* **12**, 521–531 (2018).

17. I. V. Meglinski, S. J. Matcher, Quantitative assessment of skin layers absorption and skin reflectance spectra simulation in the visible and near-infrared spectral regions. *Physiol. Meas.* **23**, 741–753 (2002).

18. T. G. Zimmerman, Personal area networks: Near-field intrabody communication. *IBM Syst. J.* **35**, 609–617 (1996).

19. S. Il Chang, K. Alashmouny, M. McCormick, Y. C. Chen, E. Yoon, BioBolt: A minimally-invasive neural interface for wireless epidural recording by intra-skin communication. *IEEE Symp. VLSI Circuits, Dig. Tech. Pap.* 146–147 (2011).

20. E. Stavrinidou, P. Leleux, H. Rajaona, D. Khodagholy, J. Rivnay, M. Lindau, S. Sanaur, G. G. Malliaras, Direct measurement of ion mobility in a conducting polymer. *Adv. Mater.* **25**, 4488–93 (2013).

21. G. Buzsáki, E. Stark, A. Berényi, D. Khodagholy, D. R. Kipke, E. Yoon, K. D. Wise, Tools for probing local circuits: High-density silicon probes combined with optogenetics. *Neuron* **86**, 92–105 (2015).

22. K. D. Harris, D. A. Henze, J. Csicsvari, H. Hirase, G. Buzsáki, Accuracy of tetrode spike separation as determined by simultaneous intracellular and extracellular measurements. *J. Neurophysiol.* **84**, 401–14 (2000).

23. J. J. Jun, N. A. Steinmetz, J. H. Siegle, D. J. Denman, M. Bauza, B. Barbarits, A. K. Lee, C. A. Anastassiou, A. Andrei, Ç. Aydın, M. Barbic, T. J. Blanche, V. Bonin, J. Couto, B. Dutta, S. L. Gratiy, D. A. Gutnisky, M. Häusser, B. Karsh, P. Ledochowitsch, C. M. Lopez, C. Mitelut, S. Musa, M. Okun, M. Pachitariu, J. Putzeys, P. D. Rich, C. Rossant, W. Sun, K. Svoboda, M. Carandini, K. D. Harris, C. Koch, J. O'Keefe, T. D. Harris, Fully integrated silicon probes for high-density recording of neural activity. *Nature* **551**, 232–236 (2017).

24. D. Khodagholy, J. N. Gelinas, T. Thesen, W. Doyle, O. Devinsky, G. G. Malliaras, G. Buzsáki, NeuroGrid: Recording action potentials from the surface of the brain. *Nat. Neurosci.* **18**, 310–315 (2015).

25. B. Lee, M. N. Zubair, Y. D. Marquez, D. M. Lee, L. A. Kalayjian, C. N. Heck, C. Y. Liu, A single-center experience with the NeuroPace RNS system: A review Of techniques and potential problems. *World Neurosurg.* **84**, 719–726 (2015).

26. B. C. Jobst, R. Kapur, G. L. Barkley, C. W. Bazil, M. J. Berg, G. K. Bergey, J. G. Boggs, S. S. Cash, A. J. Cole, M. S. Duchowny, R. B. Duckrow, J. C. Edwards, S. Eisenschenk, A. J. Fessler, N. B. Fountain, E. B. Geller, A. M. Goldman, R. R. Goodman, R. E. Gross, R. P. Gwinn, C. Heck, A. A. Herekar, L. J. Hirsch, D. King-Stephens, D. R. Labar, W. R. Marsh, K. J. Meador, I. Miller, E. M. Mizrahi, A. M. Murro, D. R. Nair, K. H. Noe, P. W. Olejniczak, Y. D. Park, P. Rutecki, V. Salanova, R. D. Sheth, C. Skidmore, M. C. Smith, D. C. Spencer, S. Srinivasan, W. Tatum, P. Van

Ness, D. G. Vossler, R. E. Wharen, G. A. Worrell, D. Yoshor, R. S. Zimmerman, T. L. Skarpaas, M. J. Morrell, Brain-responsive neurostimulation in patients with medically intractable seizures arising from eloquent and other neocortical areas. *Epilepsia* **58**, 1005–1014 (2017).

27. U. Topalovic, Z. M. Aghajan, D. Villaroman, S. Hiller, L. Christov-Moore, T. J. Wishard, M. Stangl, N. R. Hasulak, C. S. Inman, T. A. Fields, V. R. Rao, D. Eliashiv, I. Fried, N. Suthana, Wireless programmable recording and stimulation of deep brain activity in freely moving humans. *Neuron* **108**, 322–334.e9 (2020).

28. L. R. Hochberg, M. D. Serruya, G. M. Friehs, J. A. Mukand, M. Saleh, A. H. Caplan, A. Branner, D. Chen, R. D. Penn, J. P. Donoghue, Neuronal ensemble control of prosthetic devices by a human with tetraplegia. *Nature* **442**, 164–171 (2006).

29. M. Velliste, S. Perel, M. C. Spalding, A. S. Whitford, A. B. Schwartz, Cortical control of a prosthetic arm for self-feeding. *Nature* **453**, 1098–1101 (2008).

30. G. Buzsáki, Large-scale recording of neuronal ensembles. *Nat. Neurosci.* **7**, 446–51 (2004).

31. M. J. Morrell; RNS System in Epilepsy Study Group, Responsive cortical stimulation for the treatment of medically intractable partial epilepsy. *Neurology* **77**, 1295–1304 (2011).

32. R. W. P. King, B. S. Trembly, J. W. Strohbehn, The electromagnetic field of an insulated antenna in a conducting or dielectric medium. *IEEE Trans. Microw. Theory Tech.* **31**, 574–583 (1983).

33. D. C. Grahame, The electrical double layer and the theory of electrocapillarity. *Chem. Rev.* **41**, 441–501 (1947).

34. J. Israelachvili, *Intermolecular and Surface Forces* (Elsevier, 2011).

35. J. Li, Y. Dong, J. H. Park, J. Yoo, Body-coupled power transmission and energy harvesting. *Nat. Electron.* **4**, 530–538 (2021).

36. K. Hachisuka, T. Takeda, Y. Terauchi, K. Sasaki, H. Hosaka, K. Itao, Intra-body data transmission for the personal area network. *Microsyst. Technol.* **11**, 1020–1027 (2005).

37. J. Rosell, J. Colominas, P. Riu, R. Pallas-Areny, J. G. Webster, Skin impedance from 1 Hz to 1 MHz. *I.E.E.E. Trans. Biomed. Eng.* **35**, 649–651 (1988).

38. C. Gabriel, *Compilation of the Dielectric Properties of Body Tissues at RF and Microwave Frequencies* (King's Coll London (United Kingdom) Dept of Physics, 1996).

39. X. Cui, D. C. Martin, Electrochemical deposition and characterization of poly(3,4-ethylenedioxythiophene) on neural microelectrode arrays. *Sens. Actuators B* **89**, 92–102 (2003).

40. K. Tybrandt, I. V. Zozoulenko, M. Berggren, Chemical potential–electric double layer coupling in conjugated polymer–polyelectrolyte blends. *Sci. Adv.* **3**, eaao3659 (2017).

41. D. Khodagholy, T. Doublet, P. Quilichini, M. Gurfinkel, P. Leleux, A. Ghestem, E. Ismailova, T. Hervé, S. Sanaur, C. Bernard, G. G. Malliaras, In vivo recordings of brain activity using organic transistors. *Nat. Commun.* **4**, 1575 (2013).

42. International Commission on Non-Ionizing Radiation Protection (ICNIRP), Guidelines for limiting exposure to electromagnetic fields (100 kHz to 300 GHz). *Health Phys.* **118**, 483–524 (2020).

43. P. Jastrzebska-Perfect, G. D. Spyropoulos, C. Cea, Z. Zhao, O. J. Rauhala, A. Viswanathan, S. A. Sheth, J. N. Gelinas, D. Khodagholy, Mixed-conducting particulate composites for soft electronics. *Sci. Adv.* **6**, eaaz6767 (2020).

44. Z. Zhao, C. Cea, J. N. Gelinas, D. Khodagholy, Responsive manipulation of neural circuit pathology by fully implantable, front-end multiplexed embedded neuroelectronics. *Proc. Natl. Acad. Sci.* **118**, e2022659118 (2021).

45. D. Khodagholy, J. Rivnay, M. Sessolo, M. Gurfinkel, P. Leleux, L. H. Jimison, E. Stavrinidou, T. Herve, S. Sanaur, R. M. Owens, G. G. Malliaras, High transconductance organic electrochemical transistors. *Nat. Commun.* **4**, 2133 (2013).

46. S. Il Park, D. S. Brenner, G. Shin, C. D. Morgan, B. A. Copits, H. U. Chung, M. Y. Pullen, K. N. Noh, S. Davidson, S. J. Oh, J. Yoon, K. I. Jang, V. K. Samineni, M. Norman, J. G. Grajales-Reyes, S. K. Vogt, S. S. Sundaram, K. M. Wilson, J. S. Ha, R. Xu, T. Pan, T. Il Kim, Y. Huang, M. C.

Montana, J. P. Golden, M. R. Bruchas, R. W. Gereau, J. A. Rogers, Soft, stretchable, fully implantable miniaturized optoelectronic systems for wireless optogenetics. *Nat. Biotechnol.* **33**, 1280–1286 (2015).

47. C. Cea, G. D. Spyropoulos, P. Jastrzebska-Perfect, J. J. Ferrero, J. N. Gelinas, D. Khodagholy, Enhancement-mode ion-based transistor as a comprehensive interface and real-time processing unit for in vivo electrophysiology. *Nat. Mater.* **19**, 679–686 (2020).

48. A. Burton, S. M. Won, A. K. Sohrabi, T. Stuart, A. Amirhossein, J. U. Kim, Y. Park, A. Gabros, J. A. Rogers, F. Vitale, A. G. Richardson, P. Gutruf, Wireless, battery-free, and fully implantable electrical neurostimulation in freely moving rodents. *Microsyst. Nanoeng.* **7**, 62 (2021).

49. E. J. Fuller, S. T. Keene, A. Melianas, Z. Wang, S. Agarwal, Y. Li, Y. Tuchman, C. D. James, M. J. Marinella, J. J. Yang, A. Salleo, A. A. Talin, Parallel programming of an ionic floating-gate memory array for scalable neuromorphic computing. *Science* **364**, 570–574 (2019).

50. D. K. Piech, J. E. Kay, B. E. Boser, M. M. Maharbiz, *2017 39th Annual International Conference of the IEEE Engineering in Medicine and Biology Society (EMBC)* (IEEE, 2017), pp. 221–225.

51. J. Lee, V. Leung, A. H. Lee, J. Huang, P. Asbeck, P. P. Mercier, S. Shellhammer, L. Larson, F. Laiwalla, A. Nurmikko, Neural recording and stimulation using wireless networks of microimplants. *Nat. Electron.* **4**, 604–614 (2021).

52. M. Yin, M. Ghovanloo, A low-noise clockless simultaneous 32-channel wireless neural recording system with adjustable resolution. *Analog Integr. Circuits Signal Process.* **66**, 417–431 (2011).

53. H. Miranda, V. Gilja, C. A. Chestek, K. V. Shenoy, T. H. Meng, HermesD: A high-rate long-range wireless transmission system for simultaneous multichannel neural recording applications. *IEEE Trans. Biomed. Circuits Syst.* **4**, 181–191 (2010).

54. A. M. Sodagar, G. E. Perlin, Y. Yao, K. D. Wise, K. Najafi, *An Implantable Microsystem for Wireless Multi-Channel Cortical Recording* (IEEE, 2007), pp. 69–72.

55. S. Imani, A. J. Bandodkar, A. M. V. Mohan, R. Kumar, S. Yu, J. Wang, P. P. Mercier, A wearable chemical–electrophysiological hybrid biosensing system for real-time health and fitness monitoring. *Nat. Commun.* **7**, 11650 (2016).

56. H. Ando, K. Takizawa, T. Yoshida, K. Matsushita, M. Hirata, T. Suzuki, Wireless multichannel neural recording with a 128-Mbps UWB transmitter for an implantable brain-machine interfaces. *IEEE Trans. Biomed. Circuits Syst.* **10**, 1068–1078 (2016).

57. R. Muller, H.-P. Le, W. Li, P. Ledochowitsch, S. Gambini, T. Bjorninen, A. Koralek, J. M. Carmena, M. M. Maharbiz, E. Alon, A minimally invasive 64-channel wireless μECoG implant. *IEEE J. Solid-State Circuits.* **50**, 344–359 (2014).

58. R. R. Harrison, R. J. Kier, C. A. Chestek, V. Gilja, P. Nuyujukian, S. Ryu, B. Greger, F. Solzbacher, K. V. Shenoy, Wireless neural recording with single low-power integrated circuit. *IEEE Trans. Neural Syst. Rehabil. Eng.* **17**, 322–329 (2009).

59. M. Rizk, I. Obeid, S. H. Callender, P. D. Wolf, A single-chip signal processing and telemetry engine for an implantable 96-channel neural data acquisition system. *J. Neural Eng.* **4**, 309–321 (2007).

60. W. Biederman, D. J. Yeager, N. Narevsky, A. C. Koralek, J. M. Carmena, E. Alon, J. M. Rabaey, A fully-integrated, miniaturized (0.125 mm^2) 10.5 μW wireless neural sensor. *IEEE J. Solid-State Circuits.* **48**, 960–970 (2013).

61. G. Gagnon-Turcotte, A. A. Kisomi, R. Ameli, C.-O. D. Camaro, Y. LeChasseur, J.-L. Néron, P. B. Bareil, P. Fortier, C. Bories, Y. De Koninck, A wireless optogenetic headstage with multichannel electrophysiological recording capability. *Sensors* **15**, 22776–22797 (2015).

62. H. U. Chung, B. H. Kim, J. Y. Lee, J. Lee, Z. Xie, E. M. Ibler, K. Lee, A. Banks, J. Y. Jeong, J. Kim, C. Ogle, D. Grande, Y. Yu, H. Jang, P. Assem, D. Ryu, J. W. Kwak, M. Namkoong, J. Bin Park, Y. Lee, D. H. Kim, A. Ryu, J. Jeong, K. You, B. Ji, Z. Liu, Q. Huo, X. Feng, Y. Deng, Y. Xu, K.-I. Jang, J. Kim, Y. Zhang, R. Ghaffari, C. M. Rand, M. Schau, A. Hamvas, D. E. Weese-Mayer, Y. Huang, S. M. Lee, C. H. Lee, N. R. Shanbhag, A. S. Paller, S. Xu, J. A. Rogers, Binodal,

wireless epidermal electronic systems with in-sensor analytics for neonatal intensive care. *Science* **363**, eaau0780 (2019).

63. N. Ahmadi, M. L. Cavuto, P. Feng, L. B. Leene, M. Maslik, F. Mazza, O. Savolainen, K. M. Szostak, C.-S. Bouganis, J. Ekanayake, *2019 9th International IEEE/EMBS Conference on Neural Engineering (NER)* (IEEE, 2019), pp. 719–724.